Astron. Astrophys. 363, 887–900 (2000)

ASTRONOMY AND ASTROPHYSICS

High frequency peakers

I. The bright sample

D. Dallacasa[1,2], **C. Stanghellini**[3], **M. Centonza**[1,2], **and R. Fanti**[4,2]

[1] Dipartimento di Astronomia, Via Ranzani 1, 40127 Bologna, Italy
[2] Istituto di Radioastronomia – CNR, Via Gobetti 101, 40129 Bologna, Italy
[3] Istituto di Radioastronomia – C. P. 169, 96017 Noto (SR), Italy
[4] Dipartimento di Fisica, Via Irnerio 46, 40126 Bologna, Italy

Received 11 July 2000 / Accepted 9 October 2000

Abstract. Here we present a sample of sources with convex radio spectra peaking at frequencies above a few GHz. We call these radio sources High Frequency Peakers (HFPs). This sample extends to higher turnover frequencies than the samples of Compact Steep Spectrum (CSS) and GHz Peaked Spectrum (GPS) radio sources. HFPs are rare due to the strong bias against them caused by their turnover occurring at frequencies about one order of magnitude higher than in CSS-GPS samples.

The sample has been selected by a comparison between the Green Bank survey (87GB) at 4.9 GHz and the NRAO VLA Sky Survey (NVSS) at 1.4 GHz. Then the candidates have been observed with the VLA at 1.365, 1.665, 4.535, 4.985, 8.085, 8.485, 14.96 and 22.46 GHz in order to derive a simultaneous radio spectrum, and remove variable sources from the sample. The final list of genuine HFP sources consists of 55 objects with flux density exceeding 300 mJy at 4.9 GHz at the time of the 87GB observation. Optical identifications are available for 29 of them; 24 are high redshift quasars, 3 are galaxies (one of them has indeed broad lines in the optical spectrum) and 2 are BL Lac objects. The remaining sources are mostly empty fields (17) on the digitised POSS or have uncertain classification (9).

Key words: galaxies: active – radio continuum: galaxies – galaxies: quasars: general

1. Introduction

GHz-Peaked Spectrum and Compact Steep Spectrum radio sources are identified with both galaxies and quasars; however the latter are likely to represent a different phenomenon (Stanghellini et al. 1996; Snellen et al. 1999), and at least partially affected by Doppler boosting (Fanti et al. 1990) as can be inferred also by their pc-scale radio morphologies, generally more similar to those found in flat spectrum, variable sources. However a few quasars have radio structures similar to those found for CSS/GPS galaxies (Dallacasa et al. 1995; Stanghellini et al. 1997b).

Send offprint requests to: Daniele Dallacasa (ddallaca@ira.bo.cnr.it)

The pc-scale radio morphology derived from VLBI observations can be used to evaluate the effects of Doppler boosting, that is likely to play a role in sources dominated by a single, unresolved component, in which a combination of opacity effects and speed of the plasma flow might produce peaked radio spectra (see Snellen 1997; Snellen et al. 1999). Sources with their radio axis close to the plane of the sky instead are characterised by a weak core accounting for a small fraction of the total flux density.

In the framework of individual, powerful radio $galaxy$ growth, GPS and then CSS radio sources are nowadays considered the early stages, as the radio emitting region grows and expands within the interstellar matter of host galaxy, before plunging into the intergalactic medium to originate the extended radio source population (Fanti et al. 1995; Readhead et al.1996; Begelman 1996; Snellen et al. 2000). Their radio structure is dominated by jets, lobes and hot-spots, while the cores generally account for a relatively small fraction of the total flux density. The morphologies are reminiscent of the FR II radio galaxy class, and they also share the same radio power range.

It has been shown (Owsianik & Conway 1998; Owsianik at al. 1998) that in the small double lobed Compact Symmetric Objects (CSOs) the projected separation speed of the outer edges (hot-spots) is about 0.2c, confirming this hypothesis. The dynamical age of sources of about 50-100 pc in size is of the order of 10^3 yr. The estimates of the radiative ages of the small radio sources are consistent with the hypothesis that they are young (Murgia et al. 1999).

There is a correlation between (projected) linear size and turnover frequency (O'Dea 1998). As the radio source expands the turnover moves to lower frequencies as the result of a decreased energy density within the radio emitting region. The turnover in the radio spectrum is either due to synchrotron self-absorption within the small radio emitting regions or to free-free absorption in the ionised region surrounding the radio source. In some cases it is also possible that a combination of these two effects is required.

The samples of powerful CSS and GPS radio sources studied so far (e.g. Fanti et al. 1990; Stanghellini et al. 1998) list the

brightest sources with turnover frequencies ranging from about 100 MHz to about 5 GHz. The same distribution in peak frequency can be found in the samples of somewhat less powerful objects by Snellen et al. (1998) and Marecki et al. (1999).

A sample of objects with turnover frequencies above 5 GHz would represent $smaller$ and therefore $younger$ radio sources. We call these sources "High Frequency Peakers" (HFPs). They are rarely found in CSS and GPS samples since their spectral turnover occurring between a few and a few tens of GHz, generally makes them relatively weak at the frequencies where radio catalogues are available.

This class of sources also plays an important role when considering the contribution of discrete sources to the Cosmic Microvawe Backgorund (CMB) (De Zotti et al. 2000). The density and the power of the HFP sources have to be taken into serious account in space missions like MAP and PLANCK aiming to produce high resolution and high sensitivity (μK) images of the CMB radiation.

2. Candidate high frequency peakers

CSS and GPS sources have convex radio spectra peaking at frequencies ranging from about hundred MHz to a few GHz; we assume/define that HFPs have similar spectral properties, with the peak occurring at a few GHz or higher frequencies.

The availability of large areas covered by radio surveys, and the need of a spectral peak at high frequencies made the choice of the NVSS (Condon et al. 1998) and of the 87GB (Gregory et al. 1996) catalogues quite natural.

We cross correlated the 87GB catalogue at 4.9 GHz with the NVSS catalogue at 1.4 GHz and selected the sources with inverted spectra, and in particular those with a slope steeper than -0.5 ($S \propto \nu^{-\alpha}$). We defined **two** samples of candidates: the "**bright**" sample, with sources brighter than 300 mJy at 5 GHz and covering nearly the whole area of the 87GB (declination between 0 and +75°), excluding objects with $\mid b_{II} \mid < 10^{\circ}$ to avoid the galactic plane and ease the optical identification work; the "**faint**" sample is restricted to the area covered by the FIRST survey (Becker et al. 1995) as well, and limited to sources brighter than 50 mJy at 4.9 GHz. This work presents the "bright" sample, while a forthcoming paper (Stanghellini et al. 2001) will describe the "faint" sample.

The search for candidates for the bright sample started with the 1795 sources from the 87GB stronger than 300 mJy and in the region of the sky described above. We used a simple fortran program to make a cross correlation of the positions of these sources with the catalogue derived from the NVSS. The error in the position for the sources in the 87GB is much larger than that associated with the NVSS, and is generally of the order of 10-15 arcseconds in both RA and DEC. We considered positionally coincident the sources with difference in either coordinate (Δ_{RA} or Δ_{DEC}) smaller than the largest between 45 arcsec and 3 times the error reported in the 87GB catalogue. Only 55 sources could not be identified (3.1%) since they fall in areas not yet covered by our release of the NVSS catalogue (as of July, 1999). Among the remaining 1740 objects, 164 (9.4%) had an inverted spectra with slope steeper than -0.5 and they were included in our starting list. We then inspected the NVSS images to make sure that the component in the catalogue accounted for the whole flux density. The extended objects (typically FRII and a few FRI or complex radio sources), resolved by the NVSS but a single source in the 87GB, were removed. Our list of "bright" HFP candidates consisted of 103 sources. After a search for optical identification one source have been dropped, since it is associated with a planetary nebula (J1812+0651), hence to a completely different physical phenomenon. Therefore, the final list is made up with 102 (5.9% of the starting dataset) candidates and is presented in Table 1: Column 1 gives the J2000 name; Columns 2 and 3 provide the J2000 coordinates from the NVSS catalogue (very accurate positions can be found in the Jodrell Bank VLA Astrometric Survey, JVAS catalogue; Patnaik et al. 1992; Browne et al. 1998; Wilkinson et al. 1998); Columns 4, 5 and 6 report the flux densities in the NVSS, 87GB and JVAS catalogues, respectively; Column 7 shows the spectral index between the NVSS and the 87GB; Column 8 reports whether the source belongs to other relevant samples (see below); Columns 9, 10 and 11 give the optical ID, magnitude and redshift; finally Column 12 provides the B1950 source name.

We found 14 sources in common with the new GPS candidate starting list in Marecki et al. (1999) ('m' in Column 8), three objects are in the 'bright' GPS sample from Stanghellini et al. (1998) ('st'), two sources in the 'faint' GPS sample from Snellen et al. (1998) ('sn'). It has been useful to compare our list to the 550 compact extragalactic objects in Kovalev et al. (1999) ('K'), where nearly simultaneous radio spectra are available between 1 and 22 GHz. We searched our HFP candidates in the Caltech-Jodrell Bank flat-spectrum sample (Taylor et al. 1996 and references therein) ('pr', 'cj1' and 'cj2') and with the Kellermann et al. (1998) ('k') VLBA survey at 15 GHz, in order to have images of the pc-scale radio morphology. Finally most of our HFP candidates have very short snapshot images in the VLBA Calibrator Survey (VCS, Peck & Beasley 1998).

The optical ID (capitals) and redshift are from the NED database, when available. We also report our optical ID on the digitised red plates of the Palomar Observatory Sky Survey (POSS) (small 'g' and 's' for extended or stellar) when no other optical information is available; a '?' following the optical identification means that the classification is uncertain. We remark that the optical magnitudes, mostly from the NED database, reported in Table 1 are not homogeneous (i.e. in the same band). Also variability plays an important role, given that a significant fraction of the sources are associated with blazars. In fact among the candidates there are also 3 BL Lac objects from the 1 Jy sample (Stickel et al. 1991) and a few other sources known to be variable.

3. The simultaneous radio spectra

Simultaneous multifrequency observations are necessary to remove flat spectrum variable sources from the sample; in fact our selection criteria are based on two observations at 4.9 and 1.4 GHz taken a few years apart. Variable sources that happened to

Table 1. Candidates observed with the VLA. All columns are self-explicative, except Column 8, where a reference to other samples is reported; a full description is given in the text.

J2000 Name	R.A.(J2000) h m s	Dec.(J2000) d m s	$NVSS$ mJy	$87GB$ mJy	$JVAS$ mJy	$\alpha_{1.4}^{4.9}$	Other sampl.	ID		z	B1950 Name
0003+2129	00 03 19.34	21 29 44.5	83.7	352	259	-1.17					0000+212
0005+0524	00 05 20.21	05 24 10.1	127.1	300	235	-0.70		Q	16.2	1.887	0002+051
0037+1109	00 37 26.02	11 09 50.4	235.4	456	232	-0.54					0034+108
0037+0808	00 37 32.15	08 08 12.6	96.9	320		-0.97					0034+078
0039+1411	00 39 39.63	14 11 58.0	266.3	504	386	-0.52					0037+139
0107+2611	01 07 47.88	26 11 10.1	189.7	364	323	-0.53					0105+259
0111+3906	01 11 37.31	39 06 27.6	429.0	1321	830	-0.92	pr,st,K	G	22.0	0.668	0108+388
0116+2422	01 16 33.47	24 22 14.8	154.8	457	226	-0.88					0113+241
0132+4325	01 32 44.00	43 25 32.0	150.9	347	235	-0.68	cj2,m	S	18.7		0129+431
0205+1444	02 05 13.11	14 44 32.2	197.8	365	180	-0.50					0202+145
0217+0144	02 17 48.93	01 44 48.9	750.8	1608	1176	-0.62		Q	18.3	1.715	0215+015
0254+3931	02 54 42.77	39 31 33.5	199.3	408	367	-0.58	cj2,m	G	17.0	0.289	0251+393
0310+3814	03 10 49.95	38 14 53.5	236.9	760	453	-0.95	cj2,m	Q	18.5	0.816	0307+380
0312+0133	03 12 43.56	01 33 17.1	459.6	1033	474	-0.66		Q	18.2	0.664	0310+013
0313+0228	03 13 13.36	02 28 34.9	174.8	322	127	-0.50		g?	20.1		0310+022
0329+3510	03 29 15.35	35 10 08.1	262.4	545	408	-0.60					0326+349
0357+2319	03 57 21.63	23 19 53.5	176.6	327	340	-0.50					0354+231
0424+0036	04 24 46.84	00 36 06.6	493.5	1118	288	-0.67	K	BL	17.0	0.310	0422+004
0428+3259	04 28 05.82	32 59 52.0	152.3	589	509	-1.10					0424+328
0509+0541	05 09 25.96	05 41 35.7	536.4	1026	684	-0.53		S	15.3		0506+056
0519+0848	05 19 10.77	08 48 57.0	202.8	420	160	-0.59					0516+087
0530+1331	05 30 56.43	13 31 55.2	1556.7	2995	3110	-0.53	k,K	Q	20.0	2.060	0528+134
0559+5804	05 59 13.39	58 04 03.9	392.3	906	501	-0.68	cj2	Q	18.0	0.904	0554+580
0625+4440	06 25 18.27	44 40 01.7	122.7	369	183	-0.90	m	BL			0621+446
0638+5933	06 38 02.85	59 33 22.2	254.2	482	553	-0.52	cj2				0633+595
0642+6758	06 42 04.23	67 58 35.5	192.9	499	436	-0.77	cj2	Q	16.5	3.180	0636+680
0646+4451	06 46 32.09	44 51 16.8	452.8	1191	2184	-0.79	cj1,k	Q	18.5	3.396	0642+449
0650+6001	06 50 31.21	60 01 44.5	472.7	920	753	-0.54	cj1	Q	18.9	0.455	0646+600
0655+4100	06 55 10.03	41 00 10.6	226.1	425	373	-0.51	cj2,m	G	14.6	0.02156	0651+410
0722+3722	07 22 01.26	37 22 28.6	150.2	306	234	-0.58	m	s	17.5		0718+374
0733+0456	07 33 57.45	04 56 14.1	219.3	555	232	-0.76		g?	19.5		0731+050
0811+0146	08 11 26.68	01 46 54.5	535.8	1469	1310	-0.82	k,K	BL	17.5		0808+019
0831+0429	08 31 48.88	04 29 38.5	1155.9	2136	1235	-0.50	k,K	BL	16.5	0.180	0829+046
0854+0720	08 54 35.08	07 20 24.2	136.7	309	166	-0.66					0851+075
0927+3902	09 27 03.03	39 02 20.7	2885.1	7480	8012	-0.78	k,pr,K	Q	17.9	0.6948	0923+392
0958+6533	09 58 47.22	65 33 54.2	729.9	1417	1206	-0.54		BL	16.7	0.368	0954+658
1016+0513	10 16 03.11	05 13 03.5	401.7	745	303	-0.50		S	20.0		1013+054
1018+0530	10 18 27.82	05 30 29.8	278.3	652	295	-0.69		S	20.5		1015+057
1033+0711	10 33 34.00	07 11 26.2	155.9	364	216	-0.69		Q	...	1.535	1030+074
1045+0624	10 45 52.74	06 24 36.2	157.3	457	397	-0.87		Q	17.9	1.507	1043+066
1048+7143	10 48 27.56	71 43 35.2	736.8	2410	1259	-0.96	cj1	Q	19.0	1.150	1044+719
1056+7011	10 56 53.70	70 11 46.0	310.9	675	603	-0.63	cj1	Q	18.5	2.492	1053+704
1146+3958	11 46 58.31	39 58 34.9	331.4	739	565	-0.65	cj1,K	Q	18.0	1.088	1144+402
1148+5254	11 48 56.63	52 54 25.7	93.4	304	597	-0.96	cj2	Q	15.5	1.632	1146+531
1209+4119	12 09 22.81	41 19 41.0	274.2	515	486	-0.51	cj2,m	S	16.3		1206+416
1228+3706	12 28 47.40	37 06 12.0	383.8	953	868	-0.74	cj2	G	18.0	1.515	1226+373
1302+5748	13 02 52.47	57 48 37.5	321.0	758	885	-0.70	cj2	S	20.0		1300+580
1310+4653	13 10 53.61	46 53 52.2	131.0	393	361	-0.89	cj2,m	S	19.1		1308+471
1310+3233	13 10 59.45	32 33 34.9	374.3	688	605	-0.50		Q	19.2	1.650	1308+328
1335+4542	13 35 21.98	45 42 38.5	251.0	598	468	-0.71	cj1	Q	18.5	2.449	1333+459
1335+5844	13 35 25.94	58 44 00.8	292.7	820	766	-0.84	cj1				1333+589
1407+2827	14 07 00.43	28 27 14.5	817.1	2421	1939	-0.88	k,st,K	BG	16.0	0.0769	1404+286
1410+0731	14 10 35.09	07 31 21.1	192.3	362	332	-0.52					1408+077
1412+1334	14 12 36.38	13 34 38.5	196.6	399	242	-0.58					1410+138
1419+5423	14 19 46.50	54 23 15.1	733.9	1707	2187	-0.69	cj1	BL	15.7	0.151	1418+546

Table 1. (continued)

J2000 Name	R.A.(J2000) h m s	Dec.(J2000) d m s	$NVSS$ mJy	$87GB$ mJy	$JVAS$ mJy	$\alpha_{1.4}^{4.9}$	Other sampl.	ID		z	B1950 Name
1424+2256	14 24 38.13	22 56 00.6	268.4	503		-0.51		Q	16.5	3.626	1422+231
1430+1043	14 30 09.78	10 43 27.1	290.0	1236	822	-1.18	K	Q	18.5	1.710	1427+109
1457+0749	14 57 38.09	07 49 54.0	234.7	618	432	-0.79					1455+080
1458+3720	14 58 44.77	37 20 22.0	215.1	591	370	-0.82	cj2,m	G	18.2	0.333	1456+375
1505+0326	15 05 06.46	03 26 30.3	395.4	991	876	-0.75	K	Q	18.7	0.411	1502+036
1511+0518	15 11 41.18	05 18 09.3	60.6	501	502	-1.72		g	16.2	a	1509+054
1526+6650	15 26 42.88	66 50 55.0	88.3	417	312	-1.26	cj2,m	Q	17.2	3.02	1526+670
1551+5806	15 51 58.18	58 06 44.7	190.5	367	305	-0.53	cj2,m,sn	Q	15.9?	1.324	1550+582
1555+1111	15 55 43.09	11 11 24.5	312.4	636	515	-0.58		BL	15.	0.360	1553+113
1603+1105	16 03 41.93	11 05 49.0	195.5	831	357	-1.18		dss			1601+112
1616+0459	16 16 37.43	04 59 33.7	352.0	918	693	-0.78	K	Q	19.5	3.197	1614+051
1623+6624	16 23 04.44	66 24 01.0	156.0	520	287	-0.98	m,sn	G	15.1	0.203	1622+665
1645+6330	16 45 58.56	63 30 11.0	218.2	444	214	-0.58	cj2	Q	19.4	2.379	1645+635
1716+6836	17 16 13.93	68 36 38.2	489.3	988	829	-0.57	cj2	Q	18.5	0.777	1716+686
1717+1917	17 17 01.19	19 17 40.7	124.6	346	124	-0.83					1714+193
1719+0658	17 19 10.90	06 58 15.5	117.2	425	107	-1.05					1716+070
1722+6106	17 22 40.06	61 06 00.0	154.8	321	195	-0.59	m	s	19.9		1722+611
1728+1215	17 28 07.03	12 15 39.2	346.4	958	391	-0.83	K	Q	20.0		1725+123
1735+5049	17 35 49.04	50 49 11.5	432.0	798	838	-0.50	cj1	G?	23.1		1734+508
1740+2211	17 40 05.82	22 11 00.3	344.7	676	490	-0.55		g?	16.9		1737+222
1747+4658	17 47 26.68	46 58 51.0	305.1	634	871	-0.60	cj2	S	21.3		1746+470
1751+0939	17 51 32.84	09 39 01.1	623.1	2283	2058	-1.06	k,K	BL	16.8	0.322	1749+096
1800+3848	18 00 24.72	38 48 31.1	326.9	722	1177	-0.65	cj1,k,K	Q	18	2.092	1758+388
1811+1704	18 11 43.18	17 04 56.7	132.5	314	184	-0.70					1807+170
1840+3900	18 40 57.13	39 00 46.0	143.2	476	221	-0.98	cj2,m	Q	19.5	3.095	1839+389
1849+6705	18 49 15.89	67 05 40.9	517.9	992	456	-0.53	cj2	Q	20	0.657	1849+670
1850+2825	18 50 27.54	28 25 12.8	230.7	999	1467	-1.19	K	Q	17	2.560	1848+283
1855+3742	18 55 27.65	37 42 56.0	176.1	341	222	-0.54					1853+376
2021+0515	20 21 35.29	05 15 05.1	333.5	684	454	-0.58					2019+050
2024+1718	20 24 56.47	17 18 11.3	279.5	586	568	-0.60		S	17.5	1.050?	2022+171
2043+1255	20 43 10.18	12 55 14.0	221.2	429	227	-0.54					2040+127
2101+0341	21 01 38.84	03 41 32.2	590.9	1307	760	-0.65	K	Q	18	1.013	2059+034
2114+2832	21 14 58.34	28 32 57.0	396.7	773	486	-0.54		s?	19.3		2112+283
2123+0535	21 23 44.52	05 35 22.5	794.0	2523	1446	-0.94	K	Q	17.5	1.878	2121+053
2136+0041	21 36 38.56	00 41 54.5	3473.0	10467	7202	-0.90	k,st,K	Q	16.8	1.932	2134+004
2203+1007	22 03 30.95	10 07 42.9	114.6	316	235	-0.83					2201+098
2207+1652	22 07 52.79	16 52 15.6	208.9	384	280	-0.50		s?	19.7		2205+166
2212+2355	22 12 06.01	23 55 40.7	557.0	1212	723	-0.63	K	S	19.0		2209+236
2219+1806	22 19 14.05	18 06 35.4	159.2	318	357	-0.56		s?	19.0		2216+178
2219+2613	22 19 49.77	26 13 27.7	209.4	799	421	-1.09		BG	17.0	0.085	2217+259
2230+6946	22 30 36.63	69 46 27.5	509.1	1365	754	-0.80	cj1	BL?	19.5		2229+695
2241+4120	22 41 07.15	41 20 12.3	336.1	677	826	-0.57	cj2	S	17.9		2238+410
2257+0243	22 57 17.54	02 43 17.5	209.4	426	273	-0.58	K	Q	18	2.081	2254+024
2308+0946	23 08 44.18	09 46 26.2	141.6	383	120	-0.81					2306+095
2320+0513	23 20 44.83	05 13 50.5	541.9	1180	387	-0.63	K	Q	19	0.622	2318+049
2321+3204	23 21 54.84	32 04 05.6	232.9	479	179	-0.59	K	BG	17.0		2319+347
2330+3348	23 30 13.72	33 48 36.2	199.2	497	472	-0.74	K	Q	18.5	1.809	2327+335

be in a "high" activity state at the time of the 4.9 GHz observation are selected by our criteria, and need to be removed.

Hence, we have observed at the VLA the whole "bright" sample. We carried out nearly simultaneous flux density measurements at L band (with the two IFs at 1.365 and 1.665 GHz), C band (4.535 and 4.985 GHz), X band (8.085 and 8.485 GHz), U band (14.935 and 14.985 GHz) and K band (22.435 and 22.485 GHz). The observing bandwidth was chosen to be 50 MHz per IF except at 1.665 GHz, set to 25 MHz in order to avoid radio interference.

Each source was observed typically for 40 seconds at each frequency in a single snapshot, cycling through frequencies. This means that our flux density measurements are nearly simultaneous, given that they are separated by 1 minute apiece.

Table 2. VLA observations and Configurations. The total observing time (Column 3) is inclusive of the scans on the "faint" HFP candidates.

Date	Conf.	Obs. Time	code
21 Sep 1998	B	120	a
07 Nov 1998	BnC	150	b
14 Nov 1998	BnC	150	c
19 Dec 1998	C	240	d
14 Jun 1999	AnD	420	e
21 Jun 1999	AnD	180	f
25 Jun 1999	A	120	g
25 Sep 1999	A	240	h
15 Oct 1999	BnA	240	i
25 Feb 2000	BnC	240	j

For each observing run we spent one or two scans on the two primary flux density calibrators 3C286 or 3C147. Secondary calibrators were observed for 1 minute at each frequency about every 25 minutes; they were chosen aiming to minimise the telescope slewing time and therefore we could not derive accurate positions for the radio sources we observed. Accurate positions can be obtained from the JVAS catalogue (Patnaik et al. 1992; Browne et al. 1998; Wilkinson et al. 1998).

Information on the date and duration of the observing runs is summarised in Table 2. Sources from the bright and faint samples were observed together in each run in order to optimise the observing schedule.

The data reduction has been carried out following the standard procedures for the VLA implemented in the NRAO AIPS software. Separate images for each IF were obtained at L, C and X bands in order to improve the spectral coverage of our data. Imaging has been quite complicated at L band since a number of confusing sources fall within the primary beam, and an accurate flux density measurement could be obtained only once the confusing sources had been cleaned out. Generally one iteration of phase-only self-calibration have been performed before the final imaging. On the final image we perfomed a Gaussian fit by means of the task JMFIT, and also measured the source flux density with TVSTAT and IMSTAT. Generally all the HFP candidates were unresolved by the present observations; when JMFIT found some extension, it was generally much smaller than the beam size, and therefore we did not consider it.

The r.m.s. noise levels in the image plane is relevant only for measured flux densities of a few mJy, which is not the case for our sources; in fact the major contribution comes from the amplitude calibration error.

At K band, the antenna gain and atmospheric opacity vary significantly with elevation, introducing visible effects below 40°, progressively reducing the correlated flux density. Only two observing runs (19Dec98 and 14Jun99) had a few sources observed at low elevations. The flux densities were then readjusted by comparing the flux density of J0111+3906 (B0108+388), a well known supposedly non variable GPS source, observed in a run close in time.

At the end, we estimate that the overall amplitude error (1 sigma) is 3% at L,C and X bands, 5% at U band and finally 10% at K band.

4. The "bright" HFP sample

We derived the spectral indices between any pair of adjacent frequencies, and then we classified the sources into two sets: 1) the genuine HFPs, i.e. sources with peaked radio spectrum and at least a spectral index below -0.5 (55 objects) 2) flat spectrum sources (48). These objects with their flux densities are listed in Table 3 and Table 4 respectively, according to their classification.

It is interesting to note that also among these genuine HFP sources, flux density variability is not uncommon (see Sect. 7.1), and indeed 12 objects have flux densities below 300 mJy at 4.9 GHz, and at the time of our observations would have been dropped from the bright sample.

Our selection picked up also three well known GPS sources, namely J0111+3906 (G), J1407+2827 (G) and J2136+0036 (Q) (Stanghellini et al. 1998). In fact their radio spectra peak between 4 and 10 GHz.

Of the two GPS sources in Snellen et al. (1998), J1623+6624 turned out to be slightly below the 300 mJy limit, (Table 3 and Fig. 1), while J1551+5806 in our simultaneous data has a flat spectrum (Table 4 and Fig. 2) and therefore has been classified as a non-HFP source.

J1751+0939 is a well known BL Lac object from the 1Jy sample (Stickel et al. 1991), and it is classified as a HFP source. It was observed twice, and at both epochs the radio spectrum meets our selection criteria. Another BL Lac object (J0625+4440) has a genuine HFP radio spectrum. This confirms that it is possible that beamed radio sources like BL Lac objects, or more generally blazars, posses radio spectra peaking above a few GHz, as the result of a self-absorbed synchrotron emission from the jet base. The sample of HFP sources presented here is therefore expected to collect a mixture of Doppler boosted objects together with the young pregenitors of the GPS-CSS population. The determination of the pc-scale morphology will be an important tool to distinguish among these two classes.

It is interesting to analyse the the 23 sources in common with the Kovalev et al. (1999) list of compact extragalactic objects, given that they provide nearly simultaneous flux density measurements between 1 and 22 GHz, and our selection criteria can be applied in the same way. Among the 16 sources we define genuine HFPs only 11 are HFPs in Kovalev et al., while 5 would have been classified as flat spectrum sources. On the other hand, among the remaining 7 non-HFPs, 4 would be HFPs (J0424+0036, J0811+0146, J1146+3958 and J2321+3204) according to Kovalev et al. measurements. This could be due to a progressive fall off of the radio spectrum at low frequencies, since the lowest frequency in Kovalev et al. is about 40% lower than our, or to an effective variability in this class of sources, both in flux density and in spectral shape (see also Sect. 7). We would like to remark that the BL Lac object J1751+0939 is a HFP source also in Kovalev et al. data.

Table 3. Multifrequencies VLA flux densities of genuine HFP sources.

J2000 Name	Obs. code	$S_{1.4}$ mJy	$S_{1.7}$ mJy	$S_{4.5}$ mJy	$S_{5.0}$ mJy	$S_{8.1}$ mJy	$S_{8.5}$ mJy	$S_{15.0}$ mJy	$S_{22.5}$ mJy	S_{peak} Jy	ν_{peak} GHz
0003+2129	a	90	117	256	265	262	257	159	95	0.27	6.2
0005+0524	e	137	172	233	229	189	181	123	102	0.24	3.4
0037+0808	e	84	121	288	292	260	253	178	137	0.29	4.9
0111+3906	e	401	610	1353	1324	1019	972	500	300	1.37	4.2
0111+3906	f	388	584	1343	1320	994	954	500	301	1.36	4.2
0116+2422NE	a	103	130	238	243	225	220	128	87	0.24	4.9
0217+0144	e	717	841	1764	1862	2238	2262	2541	2626	>2.63	>22
0329+3510	d	391	424	764	770	733	731	638	567	0.79	5.5
0357+2319	d	257	269	535	560	605	610	628	633	>0.63	>22
0428+3259	c	149	186	484	506	539	536	421	287	0.55	7.2
0428+3259	d	161	193	468	486	525	523	416	299	0.53	7.6
0519+0848	d	183	174	141	142	179	185	292	377	>0.38	>22
0519+0848	i	175	175	251	278	378	387	491	560	>0.56	>22
0625+4440	c	194	215	418	442	535	540	563	549	0.57	14.5
0638+5933	c	260	289	569	591	670	672	693	667	0.70	12.9
0642+6758	c	232	302	485	474	375	366	251	181	0.50	3.7
0646+4451	c	432	530	1727	1896	2780	2855	3302	3199	3.29	15.5
0650+6001	c	473	598	1209	1236	1257	1250	1116	954	1.27	6.8
0655+4100	c	201	244	303	310	333	335	313	271	0.33	7.8
0722+3722	c	151	173	233	230	204	201	148	107	0.23	4.3
0722+3722	f	159	184	236	230	205	198	138	96	0.24	4.1
0927+3902	c	2859	3595	10653	11308	12992	13047	12238	10948	13.07	8.5
0927+3902	i	2772	3450	10436	10953	11990	11859	10060	8660	12.15	6.9
1016+0513	d	194	182	184	196	306	317	511	573	>0.57	>22
1016+0513	i	294	329	494	510	525	522	449	379	0.52	7.1
1045+0624	d	175	243	347	339	300	297	245	179	0.36	3.7
1045+0624	i	174	226	337	331	289	284	238	196	0.34	3.7
1148+5254	b	87	100	354	393	510	512	501	458	0.51	8.7
1335+4542	b	252	355	743	735	582	564	357	248	0.75	4.2
1335+5844	e	282	391	731	723	680	674	524	407	0.73	4.9
1407+2827	a	809	1105	2403	2398	1988	1940	1292	719	2.40	4.9
1407+2827	b	798	1096	2379	2362	2008	1966	1322	800	2.36	4.9
1407+2827	h	777	1095	2442	2426	2019	1971	1292	709	2.43	4.9
1412+1334	d	181	225	347	330	288	282	205	147	0.34	4.2
1424+2256	d	318	393	620	607	467	448	270	161	0.62	4.0
1430+1043	h	288	425	910	910	830	816	706	566	0.91	4.9
1457+0749	h	171	190	244	241	227	226	207	177	0.24	4.7
1505+0326	h	455	547	921	929	901	895	830	738	0.93	6.2
1511+0518	a	66	100	497	536	731	738	737	611	0.77	11.0
1526+6650	a	117	138	406	411	367	355	202	109	0.42	5.8
1603+1105	h	119	148	266	270	265	264	255	227	0.27	6.8
1616+0459	h	359	484	908	892	698	674	430	272	0.91	4.1
1623+6624	a	148	178	289	298	274	272	229	198	0.29	5.1
1645+6330	a	221	272	496	513	587	588	635	636	>0.64	>22
1717+1917	a	87	98	192	204	230	229	227	215	0.23	11.5
1735+5049	a	447	515	948	968	935	924	740	624	0.99	5.9
1751+0939	h	1043	1350	3252	3362	3684	3690	3691	3367	3.70	8.5
1751+0939	e	1399	1673	3525	3688	4201	4194	4178	4031	4.24	10.7
1800+3848	e	270	328	733	791	1101	1125	1364	1363	1.40	17.8
1811+1704	h	286	381	678	691	763	765	837	795	0.82	14.7
1840+3900	e	152	168	204	203	195	191	183	167	0.20	4.5
1850+2825	e	210	284	1135	1246	1561	1550	1301	1002	1.56	8.3
1855+3742	e	191	186	384	364	234	221	136	106	0.39	4.5

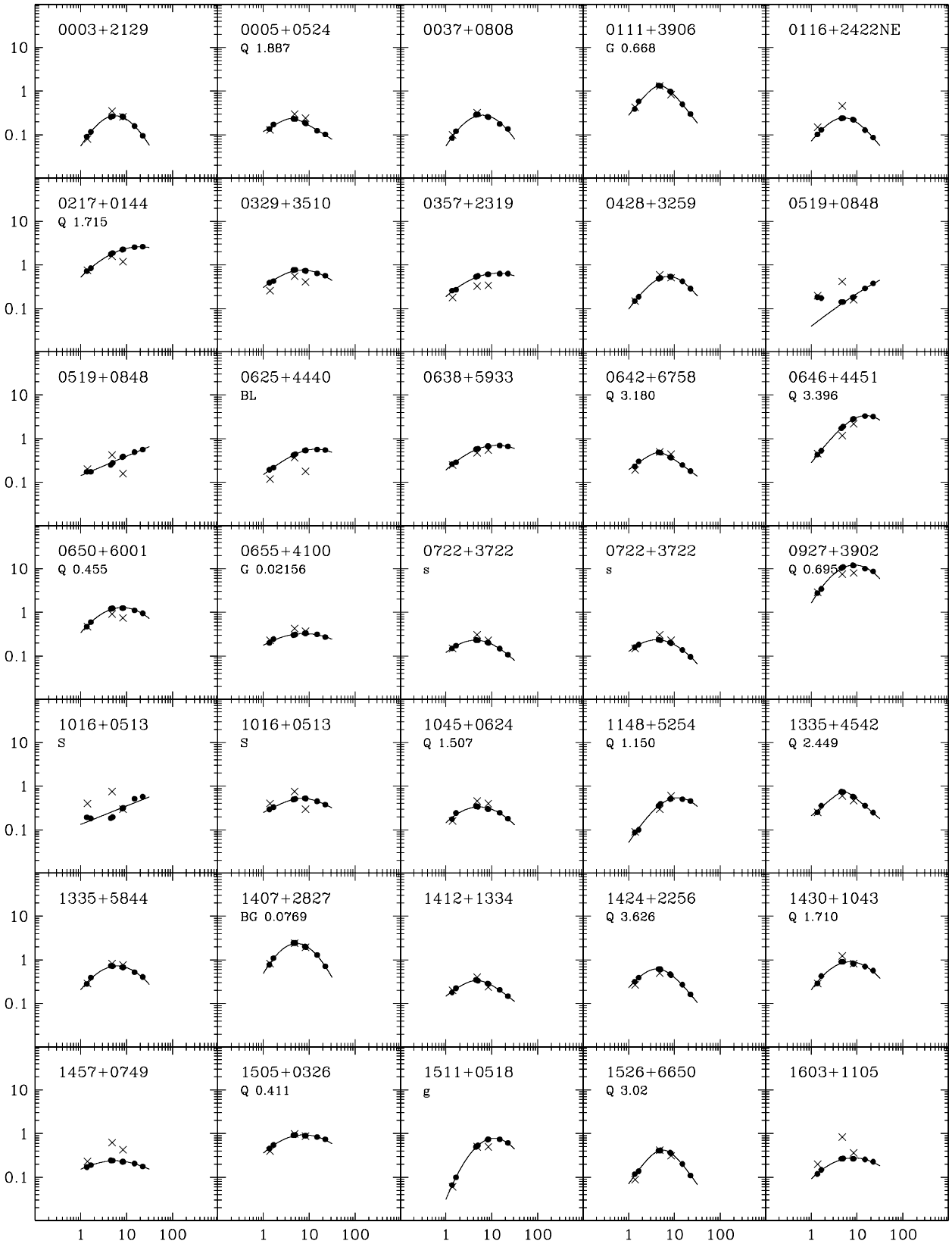

Fig. 1. Spectra of genuine HFP sources: filled circles represent the simultaneous multifrequency VLA data, while crosses are used for the flux densities from the catalogues mentioned in the text. The solid line shows the fitting curve. Log(ν) (GHz) and Log(F_ν) (Jy) are the x and y axis respectively.

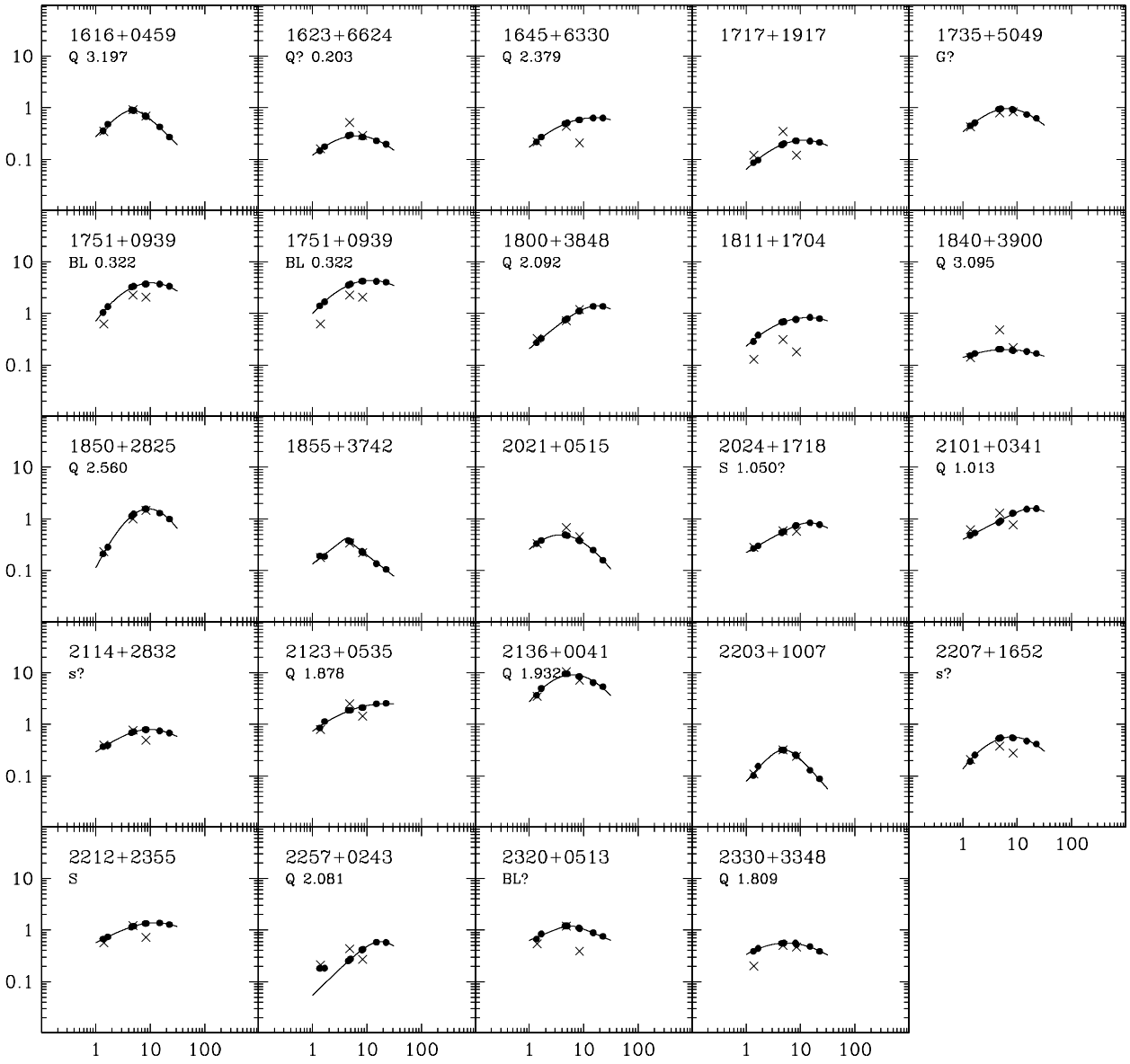

Fig. 1. (continued).

Table 3. continued)

J2000 Name	Obs. code	$S_{1.4}$ mJy	$S_{1.7}$ mJy	$S_{4.5}$ mJy	$S_{5.0}$ mJy	$S_{8.1}$ mJy	$S_{8.5}$ mJy	$S_{15.0}$ mJy	$S_{22.5}$ mJy	S_{peak} Jy	ν_{peak} GHz
2021+0515	f	331	383	492	477	387	372	251	158	0.49	3.7
2024+1718	e	268	304	544	572	740	745	838	776	0.84	14.5
2101+0341	e	481	534	854	920	1283	1298	1545	1583	>1.58	>22
2114+2832	e	371	396	691	722	797	792	749	685	0.79	9.8
2123+0535	e	861	1147	1876	1896	2121	2135	2515	2559	>2.56	>22
2136+0041	a	3682	4976	9514	9537	8532	8370	6475	5412	9.57	4.5
2136+0041	d	3478	4811	9685	9702	9129	8940	7443	6169	9.71	5.0
2203+1007	e	103	155	321	319	258	247	130	89	0.33	4.2
2207+1652	e	193	256	538	551	554	547	477	417	0.56	6.3
2212+2355	e	665	739	1141	1182	1334	1337	1374	1280	1.38	12.6
2257+0243	e	181	182	251	274	412	425	576	575	0.58	19.5
2320+0513	e	665	839	1197	1196	1088	1069	885	755	1.21	4.1
2330+3348	e	388	439	551	558	559	520	479	388	0.59	5.6

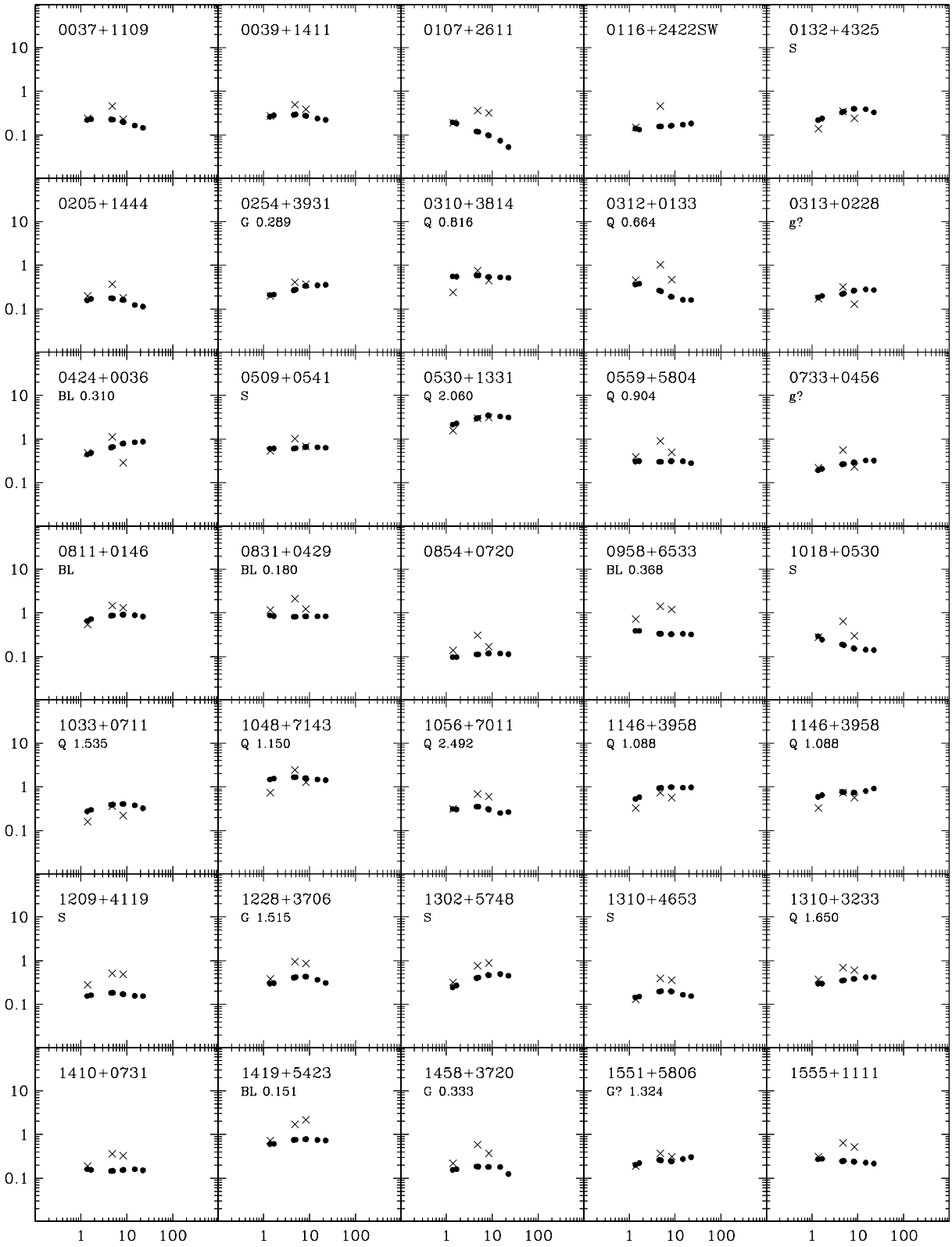

Fig. 2. Spectra of non HFP sources: as for Fig. 1, filled circles represent the simultaneous multifrequency VLA data, while crosses are used for the flux densities from the catalogues mentioned in the text. Log(ν) (GHz) and Log(F_ν) (Jy) are the x and y axis respectively.

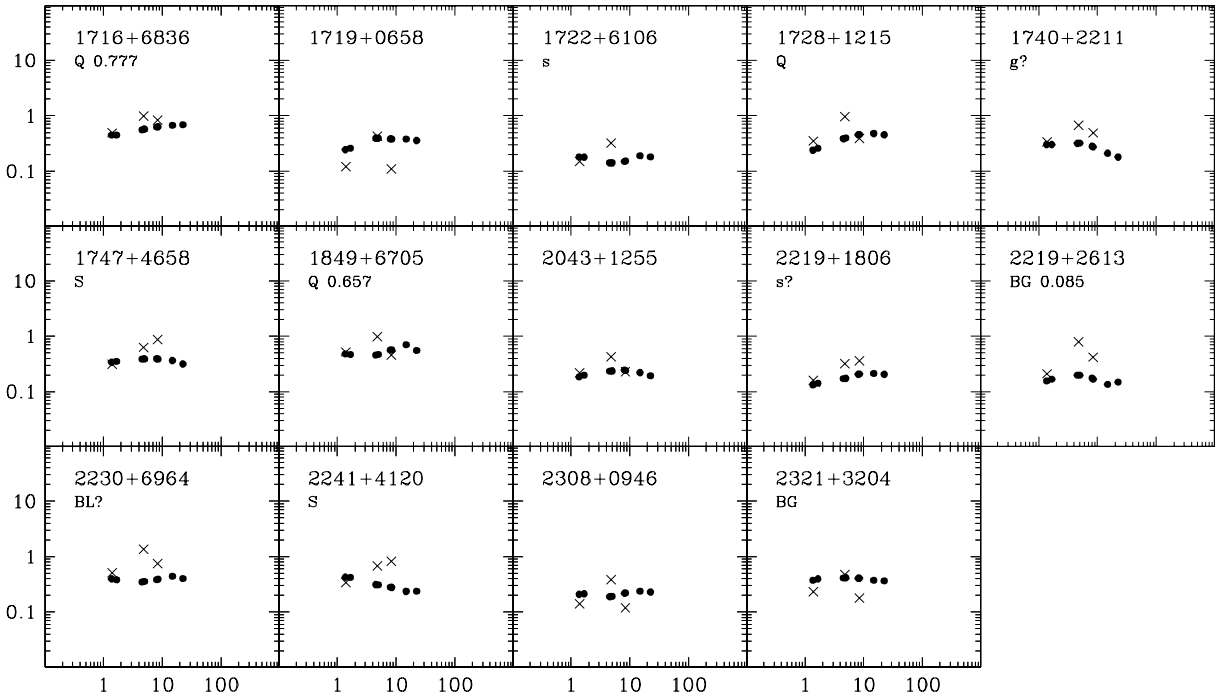

Fig. 2. (continued).

There is no clear segregation on the fraction of HFPs based on the optical identification. In fact the number of HFPs versus total is 4/9 for galaxies, 23/36 for quasars, 2/8 for BL Lacs, 16/32 for empty fields and 10/25 for objects with uncertain classification. The fractions of empty fields and identifications with an uncertain classification are still too large to allow a proper statistical analysis. An optical identification program is in progress at the 3.6m Telescopio Nazionale Galileo (TNG) in La Palma.

5. Spectral peaks

We fitted the simultaneous radio spectra of the genuine HFP sources in Table 3 in order to estimate the spectral peak and the turnover frequency. We first used the function reported as Eq. (1) in Snellen et al. (1998) or Eq. (2) in Marecki et al. (1999) in which some assumptions about the physics in the radio sources are taken into account to derive the spectral shape. However, Snellen et al. (1998) used the function only for determining the peak frequency, flux density peak and the Full Width Half Maximum of their fitted spectra. Indeed, it is well known that the description of the radio spectrum in terms of a single homogeneous synchrotron component is too simplistic, and often the parameters derived from spectral peaks can be taken as gross estimates only.

Our simultaneous radio spectra have a much better sampling and more uniform uncertainties than in Snellen et al. (1998) and Marecki et al. (1999). We tried a fit with the forementioned function, but we also fitted the radio data with a purely analytic function, with no physics behind, given it is used to determine only "analytical" quantities, namely the peak and the frequency at which it occurs. Rearranging the parameters from Kovalev et al. (1999) we used the following function:

$$\mathrm{Log}\, S = a - \sqrt{b^2 + (c\,\mathrm{Log}(\nu) - d)^2}$$

From this fitting curve we derived the spectral peak (S_m and ν_m), representing the actual maximum, regardless the point where the optical depth is unity, or any other physical measure. The parameters a, b, c and d are purely numeric, and do not provide any direct physical information.

For two sources (J0519+0848, first epoch, and J2257+0243) we excluded the two flux densities at 1.365 and 1.665 GHz in order to have a good fit of the spectral peak.

It is interesting to note note that the peak frequencies in our bright HFP sample are about a factor of 5 higher than in Snellen et al. (1998), and our spectra generally appear broader. We do not provide the FWHM of our fitted spectra since the range sampled by our simultaneous measurements is rather small, and very seldom the 22 GHz flux density falls below half the peak flux density, making the detemination of the width rather uncertain. We did not consider datapoints at low (WENSS, Rengelink et al. 1997; Texas, Douglas et al. 1996) and high frequencies (e.g. Steppe et al. 1988, 1992, 1993, 1995) since one of the key point in the selection is the simultaneous measurements at the various frequencies.

We remark further that only a few sources (namely J0217+0144, J0357+2319, J1645+6630, J2101+0341 and J2123+0535) have flux densities still rising at 22 GHz, although all of them have slopes with a spectral index close to 0. Also the first epoch of J1016+0513 has a spectral peak above 22 GHz; this source indeed possess a rather unusual radio spectrum, and also show prominent variability in both flux density and spectral shape. In fact the peak flux does not change very much but the peak frequency moves from about 22 GHz down to 7.1 GHz

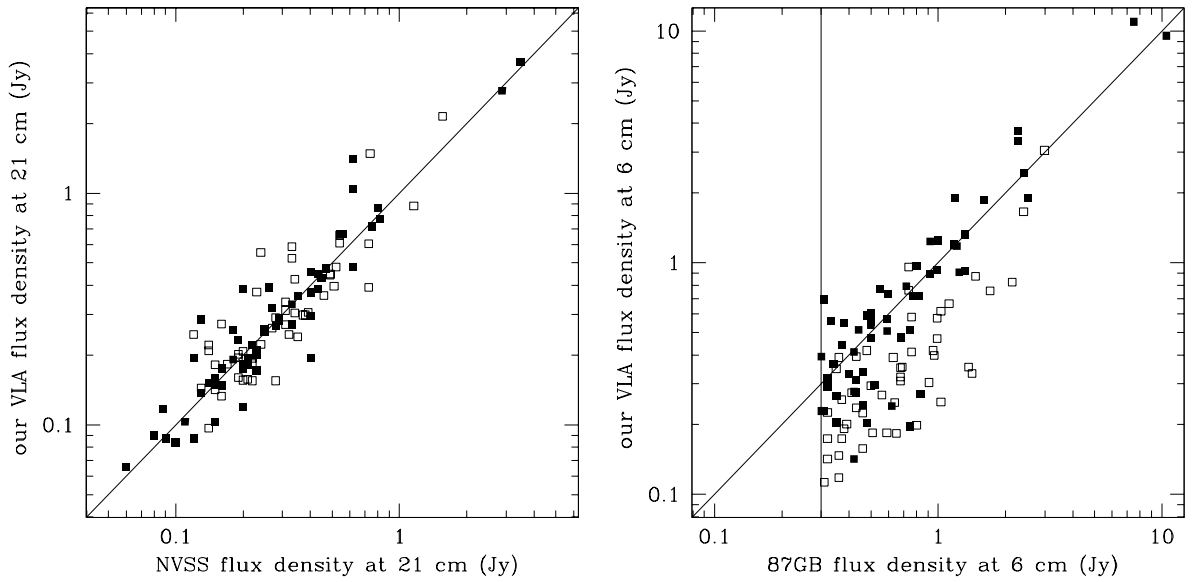

Fig. 3. Flux densities from the NVSS (*left*) and 87GB (*right*) catalogues are compared to ours at the same frequency. Filled squares represent genuine HFP sources (both "bright" and "weak", while open squares are for non HFPs.

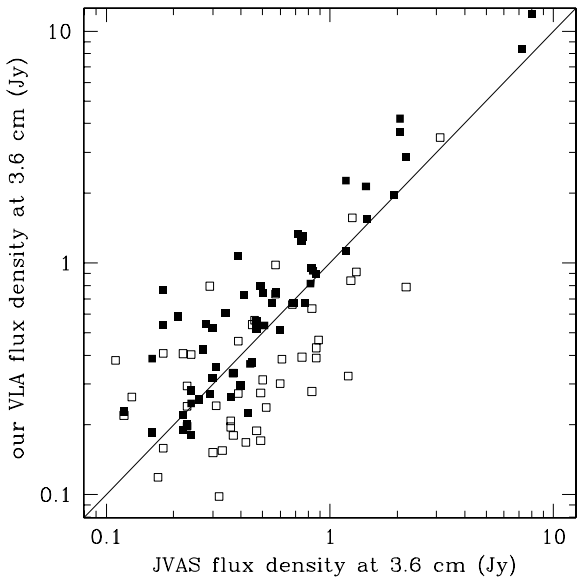

Fig. 3. (continued) Comparison between our flux density measures at 8.46 GHz with the Flux densities from the JVAS catalogue. Filled squares represent genuine HFP sources (both "bright" and "weak"), while open squares are for non HFPs.

in the second epoch; the flux density at 5.0 GHz, close to the 87GB, rises from 0.20 up to 0.51 Jy.

A spectral shape similar to the first epoch for J1016+0513 has been found in J2257+0243, whose spectral peak is 0.58 Jy at about 20 GHz, but its flux density at 4.9 GHz is only 0.27 Jy, and therefore below the 87GB limit.

GPS sources have steep optically thin radio spectra, and they are not as broad as found in the majority of our genuine HFPs. We would need observations at higher frequencies in order to study the optically thin emission, and to disentangle the contamination by beamed objects, since we do expect that beamed objects are characterised by a dominant flat spectrum component (on the pc scale), whose relative relevance increases with frequency.

6. Comparison with NVSS, 87GB and JVAS flux densities

We compared the flux densities we measured with the values from the NVSS at 1.4 GHz, from the 87GB at 4.9 GHz and also from the JVAS catalogue at 8.4 GHz, where all our candidates except J0037+0808 and J1424+2256 are included. We always considered our data at the closest frequency to that of the forementioned catalogues.

The effects due to confusion are generally marginal since we can evaluate any contribution from confusing sources in the large beam of the 87GB at 4.9 GHz from the NVSS image and also from the VLA image obtained from our data.

Only one case (J0116+2422) needs attention since there are two unresolved NVSS sources separated by about 73 arcsec in p.a. $\sim 60^{\circ}$, but within the 87GB beam. By summing the two flux densities at 1.4 GHz, the spectral index with the 87GB would have dropped the source out of the candidate sample (α =0.43). The 87GB position lies in between the two NVSS sources, at 35 arcsec from the southwestern one. However we decided to observe anyways this pair, since if one would have had a commonly steep spectrum, the other would have been inverted enough to be an HFP candidate.

Fig. 3 displays the comparisons between our flux density measurements and those from the foremetioned catalogues. We distinguished among HFP and non-HFP sources by using filled or empty squares respectively.

At 1.4 GHz the data are evenly scattered around the 1:1 relation without any evidence for a different behaviour between the two classes of HFP and non-HFP sources. If we consider

Table 4. Non HFP sources.

J2000 Name	Obs. code	$S_{1.4}$ mJy	$S_{1.7}$ mJy	$S_{4.5}$ mJy	$S_{5.0}$ mJy	$S_{8.1}$ mJy	$S_{8.5}$ mJy	$S_{15.0}$ mJy	$S_{22.5}$ mJy
0037+1109	a	223	232	228	224	203	198	164	146
0039+1411	a	262	282	290	295	279	273	239	223
0107+2611	a	195	184	121	118	99	98	74	53
0116+2422SW	a	142	133	158	158	161	165	172	183
0132+4325	e	221	240	333	348	401	402	388	332
0205+1444	e	156	170	175	174	161	159	123	113
0254+3931	f	208	212	266	275	335	334	348	355
0310+3814	d	556	545	588	584	543	542	525	512
0312+0133	e	362	377	265	250	191	189	162	159
0313+0228	e	183	198	219	226	260	264	281	272
0424+0036	e	442	484	638	667	783	794	842	873
0509+0541	d	608	609	607	616	656	663	645	632
0530+1331	c	2145	2281	2946	3056	3476	3475	3294	3120
0530+1331	i	2102	2486	2905	2876	2969	3031	3944	4428
0559+5804	f	306	313	304	304	312	313	312	283
0733+0456	d	194	208	265	268	291	295	323	322
0811+0146	d	660	722	863	875	908	913	888	828
0831+0429	d	879	850	822	823	836	838	841	839
0854+0720	d	97	97	113	113	118	119	118	114
0958+6533	c	392	390	335	333	326	325	334	322
1018+0530	d	291	244	190	183	155	152	144	141
1033+0711	d	273	298	384	390	408	406	378	322
1048+7143	b	1479	1544	1653	1656	1573	1564	1474	1419
1056+7011	b	312	306	353	352	309	302	252	263
1146+3958	b	524	576	939	958	982	980	955	971
1146+3958	i	589	644	760	759	735	735	803	912
1209+4119	b	155	162	182	184	172	171	157	154
1228+3706	b	298	304	408	418	434	430	364	307
1302+5748	e	245	270	399	412	471	464	494	454
1310+4653	b	144	152	195	201	199	196	165	154
1310+3233	d	298	298	350	354	383	385	417	422
1410+0731	d	160	155	145	147	154	155	161	152
1419+5423	j	604	610	752	756	761	763	770	760
1458+3720	g	155	161	185	184	181	180	180	125
1551+5806	h	202	222	262	256	244	242	275	304
1555+1111	a	271	280	245	249	241	238	228	216
1716+6836	a	448	449	561	575	631	634	678	692
1719+0658	h	245	260	393	393	383	379	379	359
1722+6106	a	182	179	142	142	151	154	189	181
1728+1215	h	240	260	387	397	454	459	480	453
1740+2211	a	304	303	319	322	282	275	211	180
1747+4658	e	340	350	387	390	393	389	365	316
1849+6705	f	481	471	459	470	563	567	707	555
2043+1255	e	184	199	233	236	245	241	221	193
2219+1806	e	133	141	172	174	206	208	214	206
2219+2613	e	157	167	199	199	175	168	136	148
2230+6964	e	397	381	350	355	385	392	444	403
2241+4120	e	426	420	313	309	280	279	236	238
2308+0946	a	209	213	190	192	218	220	239	230
2321+3204	a	375	397	413	418	407	408	372	368

R as the ratio between our flux density over the measure in the catalogue (NVSS, 87GB or JVAS) at about the same frequency, we find that the median of the $R_{1.4}$ distribution is 0.99 for the 55 HFPs and 0.94 for the 47 non-HFPs.

At 4.9 GHz it is clear that, on average, the 87GB flux densities exceed our measurements; it is also evident that genuine HFP and non-HFP objects behave completely different, with the former nearly randomly scattered around the 1:1 relation (the median of the $R_{4.9}$ distribution is 0.97), and the latter generally well below (the median is 0.51). As mentioned in Sect. 3, this has to be expected since our selection criteria favours the inclusion of variable sources at a high state at the time of the 87 GB observation, and therefore it is natural to find non-HFP sources in the lower right part of the panel.

At 8.4 GHz the scenario is completely different, with the non-HFP sources generally weaker in our observations than in the JVAS catalogue (the median of $R_{8.4}$is 0.71), but with the HFP sources $brighter$ (median = 1.16).

We should consider that the comparisons of the flux densities at 4.9 GHz might be somehow influenced by a different technique for the observation and by a totally different instrument, but it should not affect the class of (point) source observed. Therefore the significantly different behavior between HFPs and non-HFPs is physically relevant.

A proper statistical analysis will be carried out in a forthcoming paper where also the 'faint' sample will be considered (Stanghellini et al. 2001).

7. Discussion

Our constraints in declination and galactic latitude leave an area of 4.978 sr; however the effective area where we have searched for cross identification between the 87GB and the NVSS is 4.825 sr, if we consider that 3.1% of the sources fall in regions where the NVSS is not available as yet. We ended up with 55 genuine "bright" HFP sources and this gives a density of 11.4 sources per sr. We will discuss in more detail the source counts as a function of the limiting flux density after the selection of the "faint" HFP sample in order to span a wider flux density range, with a larger number of objects. In the framework of the "youth" model for CSS and GPS radio sources the number of CSSs/GPSs/HFPs is related to the time they spend in each stage and to the variation of the total radio luminosity with time. It is therefore very likely that the number of HFP progenitors of GPS sources is small, i.e. only a fraction of the "bright" HFP sources will indeed develop into GPS and CSS stages. A further multifrequency radio observation, the determination of the VLBI structure, the optical identification and spectroscopy will be important tools to disentangle the intrisically young radio sources from the beamed objects.

7.1. Size estimate

We have derived estimates for the component size by assuming that the radio emission is originated in a single homogenous region, and that the source is in equipartition. Following Scott & Readhead (1977) and assuming an injection index of 0.75, we derive component sizes in the range from 0.3 to 3 mas. In a similar way we have estimated the source largest size (LS) from the relation between the source size (considering the outer edges) and the turnover frequency derived by O'Dea (1998) for bright CSS and GPS sources. The values obtained cover a range between a few mas to a few tens of mas. Therefore, these objects would represent the extreme representatives of the GPS population, being on average about one order of magnitude smaller. Hence, in the framework of a radio source growing and expanding within the host galaxy, HFPs would represent the very early stage.

7.2. Flux density variability

Fig. 3, can also be used to test for flux density variability: it is rather evident that this phenomenon is common among HFP sources. This is also reinforced by the simultaneous radio spectra shown in Fig. 1 where often the NVSS, 87GB and JVAS datapoints clearly stands out with respect to our measurements.

Further, a few sources have been observed twice or more in our runs, and the case of the forementioned J1016+0513 is an example of significant variability in both spectral shape and flux density. If we assume that the spectral peak has moved from about 22 GHz down to 7.1 GHz as effect of pure expansion, the source component equipartition size would have increased by a factor of 2.9 from December 1998 to October 1999; assuming a redshift of 1.0 the size would have grown from 0.24 to 0.71 mas corresponding to 1.0 and 3.0 pc (with $H_o = 100$ km s^{-1}Mpc^{-1} and $q_o = 0.5$), and leading to an expansion velocity of 15.6c! This suggests/confirms either that a significant contamination of the HFP sample by beamed objects or that the sources are not in equipartition.

Other sources like J0927+3902, J1751+0939 and J2136+0041 only show flux density variability, without an appreciable peak frequency or shape change. Finally other sources like J0111+3906, J0428+3259, J1045+0624, J1407+2827 have turned out to have constant flux densities within the calibration errors. In particular J1407+2827 (alias OQ208 or B1404+286) has an interesting history of decrease of its flux density by about 20% at cm wavelenghts in the eighties (Stanghellini et al. 1997a), but remained stable since then.

All these results deserve a deeper investigation by means of a second VLA multifrequency observation.

8. Summary

We have presented a sample of 55 High Frequency Peakers, i.e. radio sources with radio spectra having their maxima at frequencies about an order of magnitude higher than known GPS samples. This sample is intended to provide smaller and younger radio sources, but it is also likely to contain objects with properties different from the conventional CSS-GPS class. Further work is required to complete the optical identification and redshift determination, while further multifrequency polarimetric VLA observations would provide useful insights to distinguish

subclasses within our HFP sample. The determination of the pc-scale morphology will be a key point to distinguish between "young" and beamed objects.

Another HFP sample on a restricted area but deeper by a factor of 6 in limiting flux density will be presented in a forthcoming paper (Stanghellini et al. 2001).

Acknowledgements. We acknowledge financial support from the Italian M.U.R.S.T., under the program Cofin-02-98. The National Radio Astronomy Observatory is operated by Associated Universities, Inc. under cooperative agreement with the National Science Foundation. We acknowledge the use of the NASA/IPAC Extragalactic Database (NED), which is operated by the Jet Propulsion Laboratory (JPL), California Institute of Technology, under contract with the Natiional Aeronautics and Space Administration (NASA). Finally we wish to thank the referee, Ignas Snellen, whose comments considerably improved the manuscript.

References

Becker R.H., White R.L., Helfand D.J., 1995, ApJ 450, 559
Begelman M.C., 1996, In: Carilli C.L., Harris D.E. (eds.) Proc. Cygnus A – Study of radio Galaxy. CUP, Cambridge, p. 209
Browne I.W.A., Patnaik A.R., Wilkinson P.N., Wrobel J.A., 1998, MNRAS 293, 257
Condon J.J., Cotton W.D., Greisen E.W., et al., 1998, AJ 115, 1693
Dallacasa D., Fanti C., Fanti R., et al., 1995, A&A 295, 27
De Zotti G., Granato G.L., Silva L., Maino D., Danese L., 2000, A&A 354, 467
Douglas J.N., Bash F.N., Bozyan F.A., et al., 1996, AJ 111, 1945
Fanti R., Fanti C., Schilizzi R.T., et al., 1990, A&A 231, 333
Fanti C., Fanti R., Dallacasa D., et al., 1995, A&A 302, 317
Gregory P.C., Scott W.K., Douglas K., Condon J.J., 1996, ApJS 103, 427
Kellermann K.I., Vermeulen R.C., Zensus J.A., Cohen M.H., 1998, ApJS 1125, 1318
Kovalev Y.Y., Nizhelsky N.A., Kovalev Y.A., et al., 1999, A&AS 139, 545
Marecki A., Falcke H., Niezgoda J., et al., 1999, A&AS 135, 273
Murgia M., Fanti C., Fanti R., et al., 1999, 345, 769
O'Dea C.P., 1998, PASP 110, 493
Owsianik I., Conway J.E., 1998, A&A 337, 69
Owsianik I., Conway J.E., Polatidis A.G., 1998, A&A 336, L37
Patnaik A.R., Browne I.W.A., Wilkinson P.N., Wrobel J.M., 1992, MNRAS 254, 655
Peck A.B., Beasley A.J., 1998, In: Zensus J.A., Taylor G.B., Wrobel J.M. (eds.) IAU Colloq. 164, Radio Emission from Galactic and Extragalactic Compact Sources. ASP, San Francisco, p. 144; 155
Readhead A.C.S., Taylor G.B., Pearson T.J., Wilkinson P.N., 1996, ApJ 460, 634
Rengelink R.B., Tang Y., de Bruyn A.G., et al., 1997, A&A 124, 259
Scott M.A., Readhead A.C.S., 1977, MNRAS 180, 539
Snellen I.A.G., 1997, Ph.D. Thesis, University of Leiden
Snellen I.A.G., Schilizzi R.T., de Bruyn A.G., et al., 1998, A&AS 131, 435
Snellen I.A.G., Schilizzi R.T., Bremer M.N., et al., 1999, MNRAS 307, 149
Snellen I.A.G., Schilizzi R.T., Miley G.K., et al., 2000, MNRAS in press, (astroph0002130)
Stanghellini C., Dallacasa D., O'Dea C.P., et al., 1996, In: Snellen I.A.G., Schilizzi R.T., Röttgering H.J.A., Bremer M.N. (eds.) Proc. 2nd Workshop on GPS&CSS Radio Sources, Leiden Observatory, Leiden, p. 4
Stanghellini C., Bondi M., Dallacasa D., et al., 1997a, A&A 318, 376
Stanghellini C., O' Dea C.P., Baum S.A., et al., 1997b, A&A 325, 943
Stanghellini C., O'Dea C.P., Dallacasa D., et al., 1998, A&AS 131, 303
Stanghellini C., Dallacasa D., Fanti R., 2001, in preparation
Steppe H., Salter C.J., Chini R., et al., 1988, A&AS 75, 317
Steppe H., Liechti S., Mauersberger R., et al., 1992, A&AS 96, 441
Steppe H., Paubert G., Sievers A., et al., 1993, A&AS 102, 611
Steppe H., Jeyakumar S., Saikia D.J., Salter C.J., 1995, A&AS 113, 409
Stickel M., Padovani P., Urry C.M., et al., 1991, ApJ 374, 431
Taylor G.B., Vermeulen R.C., Readhead A.C.S., et al., 1996, ApJS 107, 37
Wilkinson P.N., Browne I.W.A., Patnaik A.R., et al., 1998, MNRAS 300, 790